Applied Physics Letters ARTICLE scitation.org/journal/apl

Photonic implementation of artificial synapses in ultrafast laser inscribed waveguides in chalcogenide glass

Cite as: Appl. Phys. Lett. **119**, 031104 (2021); doi: 10.1063/5.0055067
Submitted: 25 April 2021 · Accepted: 6 July 2021 ·
Published Online: 19 July 2021

M. Ramos,[1,2,a)] V. Bharadwaj,[3,4] B. Sotillo,[3,b)] B. Gholipour,[5,c)] A. N. Giakoumaki,[3] R. Ramponi,[3] S. M. Eaton,[3] and C. Soci[2]

AFFILIATIONS

[1]ICRM, Interdisciplinary Graduate School, Nanyang Technological University, Singapore 639798, Singapore
[2]Centre for Disruptive Photonic Technologies, TPI, Nanyang Technological University, Singapore 639798, Singapore
[3]IFN-CNR, Department of Physics, Politecnico di Milano, Milano 20133, Italy
[4]Center for Nano Science and Technology, Istituto Italiano di Tecnologia, Milano 20133, Italy
[5]Optoelectronics Research Centre, University of Southampton, Southampton SO17 1BJ, United Kingdom

[a)]**Present address:** Applied Physics Department, Universidad de Alicante, Alicante 03690, Spain.
Author to whom correspondence should be addressed: mramos@ua.es
[b)]**Present address:** Department of Materials Physics, Faculty of Physics, Universidad Complutense de Madrid, Madrid 28040, Spain.
[c)]**Present address:** Nanoscale Optics Lab, Electrical and Computer Engineering Department, University of Alberta, Edmonton, Canada

ABSTRACT

Simple and direct prototyping methods are ideal for large-scale delivery of cognitive photonic hardware. Here, we choose ultrafast laser writing as a direct fabrication technique to later demonstrate all-optical synaptic-like performance along the laser-written waveguides in a chalcogenide glass. Neuronal communication protocols, such as excitatory and inhibitory responses, temporal summations, and spike-timing-dependent plasticity, are shown in the glass chip. This work manifests the potential for large-scale delivery of fully integrated photonic chips based on cognitive principles by single-step fabrication procedures.

The inefficiency of conventional electronic computers to solve large combinatorial problems has prompted the incessant search for novel computational hardware.[1,2] Alternative designs to von Neumann architectures offering memory and computation in a co-localized single unit, like in the human brain, could offer more energy-efficient platforms.[1–3] A first step toward solving this issue is finding suitable materials that can emulate synaptic functions as a response to an external stimulus, as it takes place in biological nervous systems.

Inspired by such systems, state-of-the-art neuromorphic hardware is mostly based on resistive switching memories[4–7] and transistors.[8–12] Notwithstanding the progress in pure synaptic electronics, the implementation of light waves in neural networks can overcome the limitations of electronics by offering potential benefits related to ultrafast processing speeds, large bandwidths, and improved connectivity between computing modules.[13] To develop purely photonic artificial neural networks, a set of key components capable of offering efficient interconnections (biological axons and dendrites), summations and thresholding (soma), weighting (synapse), and memory are essential. Also, artificial neuromorphic networks should offer a massively parallel and compact three-dimensional architecture that mimics the large number of neurons and synapses in the brain. The interconnection, parallelism, and compactness requisites can be achieved through the use of waveguide platforms, whereas summations, thresholding, weighting, and memory can be performed via light sources combined with materials capable of offering plasticity under certain optical conditions.

Purely photonic implementations of neuromorphic hardware have been demonstrated, including optical synapses traveling along chalcogenide fibers and waveguides,[14,15] silicon photonics based on microring resonators for network reconfiguration[16,17] or photonic parallel networks for the solution of combinatorial problems.[18–20] Also, optimization algorithms for an efficient utilization of such photonic hardware have been developed.[21] However, all the neuromorphic

hardware developed until now depends on manufacturing methods that require a tedious amount of processing steps, making the fabrication procedure time consuming. Direct and single-step prototyping techniques need to be employed for an efficient large-scale delivery of neuromorphic hardware, additionally providing portability and easy coupling mechanisms to other optical circuitry.

Here, we propose the use of femtosecond laser writing[22,23] as a direct prototyping technique to fabricate waveguides that can work as all-optical neuromorphic units. The spiking activity (action potentials) underlying in biological nervous systems is emulated in the waveguides by inducing a transient photodarkening at the waveguide's input facet upon illumination with photon energies near the bandgap of the hosting chalcogenide glass.[33] The control of the input light parameters from the optical source responsible for photodarkening allows for several intra- and inter-neuronal communication protocols at the photonic waveguides.

In this work, the gallium lanthanum sulfide (GLS) glass has been selected as the hosting platform for laser inscription of the optical waveguides. The GLS substrates used were rectangular slabs with dimensions of $(10 \times 10 \times 1)$ mm^3. Details about the synthesis of the GLS substrates are available in the previous literature.[24]

The ultrafast laser writing technique is based on laser-induced optical breakdown, entailing nonlinear absorption of the ultrashort laser pulses via a rapid electron ionization, which is confined within the focal volume, and followed by an energy transfer to the material's lattice. The footprint left in the laser-irradiated volume consists of thermally induced defects and material densification/ablation, which, in turn, give rise to refractive index changes.[23]

The micromachining system illustrated in Fig. 1(a) has been employed for waveguide inscriptions. The workstation consists of a femtosecond Yb:KGW (potassium gadolinium tungstate) oscillator (Pharos, Light Conversion) emitting at a 1030 nm wavelength, whose optical output is regeneratively amplified. The emitted pulses have a fixed pulse duration of 230 fs, and for the purpose of this work, the equipment has been configured to deliver pulses at a 500 kHz repetition rate.

The power control of the laser beam is provided by an attenuator composed of a half wave plate (HWP) and a linear polarizer (LP). The rotation of the HWP allows for the selection of the power ratio between *p*-polarized and *s*-polarized beams. The rotation of a second HWP allows for the selection of the desired laser writing polarization. The beam is then steered at a dichroic mirror presenting a high reflectivity at a narrow wavelength band around the laser emission, sending the beam to the substrate after passing through a 0.42 NA, 50× infinity-corrected microscope objective lens.

The sample stage offers displacement along three axes with a resolution of ∼1 nm. To ease the alignment of the laser spot onto the substrates, a charged-couple device is placed behind the dichroic mirror, collecting the backreflection of the focused laser beam at the substrate's top surface and providing a tracing of the waveguide writing in real time. The integration of all the components in the workstation is interfaced by a computer-controlled software. Thus, the technique offers a rapid way of manufacturing devices by modifying the algorithm that controls the movement of the translational stage.

During waveguide fabrications, a multiscan inscription modality has been adopted to reduce the effects of spherical aberration and self-focusing of light. The multiscan modality is shown in Fig. 1(b) and consists of several single laser scans at low pulse energies overlapping transversally to the overall waveguide writing direction. A reasonable balance between pulse energy and translation speed led to optimal waveguides at 70 nJ and at 5 mm/s, while 18 scans per line with a separation distance of 0.3 μm allowed for the best compromise between coupling and propagation losses. Waveguide inscriptions have been performed at a laser polarization perpendicular to the scan direction [Fig. 1(b)] and at a depth of 150 μm below the sample surface.

Following the laser fabrication of the waveguides, white-light optical microscopy in the transmission mode has been employed to observe the guiding structures formed within the bulk of the substrates. Figure 1(c) shows a type I waveguiding structure with a uniform overhead shape and a well-defined central area, indicating a positive refractive index contrast with respect to the bulk. The cross section of the corresponding waveguide is shown in Fig. 1(c), revealing an optimum mode confinement due to its rectangular shape, typical of waveguides resulting from the multiscan writing modality.

From a fiber butt-coupled characterization, the resulting waveguides present nearly Gaussian single mode guiding at a 800 nm wavelength with mode field diameters (MFDs) of 7.5 ± 0.5 μm [Fig. 1(e)].

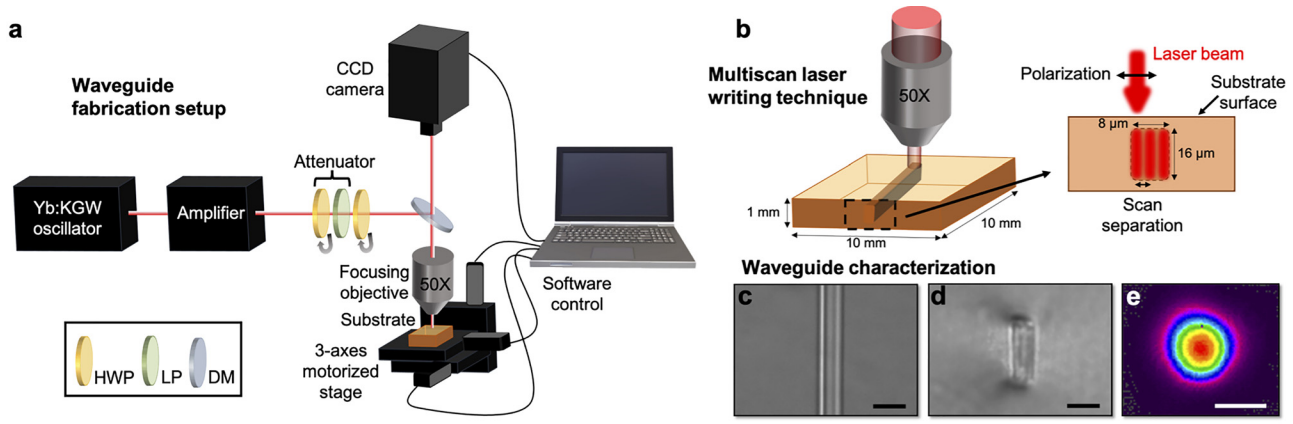

FIG. 1. (a) Laser micromachining station (HWP: half-wave plate, LP: linear polarizer, DM: dichroic mirror). (b) Multiscan laser inscription. (c)–(e) Waveguide characterization: overhead microscope image of the fabricated waveguide (c), waveguide cross section (d), waveguide guided single mode at 800 nm (e). Scale bars in (c) and (d) indicate 10 μm, while the scale bar in (e) represents 5 μm.

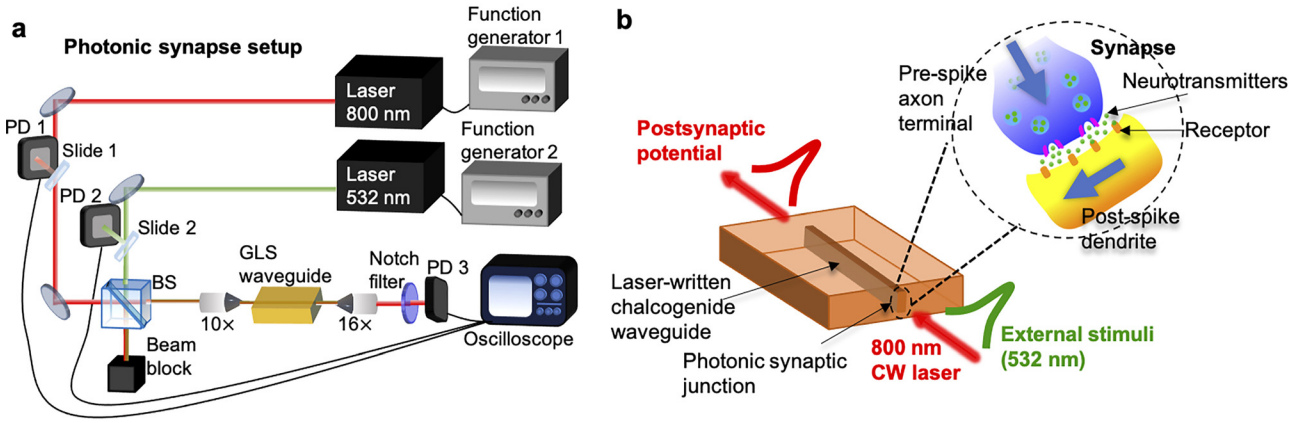

FIG. 2. (a) Experimental setup used to mimic the photonic synapse in the waveguide (PD: photodetector, BS: beam splitter). (b) Analogy between the biological and the photonic synapse. Here, the waveguide allows the generation of action potentials (spikes) at the exposure point where both laser beams meet each other (photonic synapse) and traveling all along the waveguide (photonic axon).

The fabricated waveguides have insertion losses of 2.0 dB, coupling losses of 0.7 dB/facet, and propagation losses of 0.1 dB/cm. Further information about the characterization of the waveguides is detailed in the previous work.[24]

To emulate the function of the biological synapse, two continuous-wave laser sources are externally modulated by two function generators and collinearly launched into the GLS waveguide [Fig. 2(a)]. Simultaneously, the monitoring of the laser beams is collected by the Fresnel reflection of two glass slides into two photodetectors interfaced with an oscilloscope. One of the laser beams carries photon energies below the optical gap of the pristine GLS glass ($\lambda = 800$ nm), whereas the second beam carries photon energies above the optical gap of the glass substrate ($\lambda = 532$ nm). The light source operating at $\lambda = 532$ nm is used to illuminate the waveguide's input port to induce photodarkening at the exposure point, mimicking the action of an external stimulus or a pre-spike signal in a biological neuron. On the other hand, the light at $\lambda = 800$ nm lies within the transparency wavelength range of the glass and is guided through the waveguide, delivering the post-spike function [Fig. 2(b)]. The guided light is collected at the waveguide's output and directed to a photodetector, which is connected to an oscilloscope to monitor the temporal evolution of the optical transmission along the waveguide.

The photodarkening characteristics of the laser inscribed waveguides are tested under a pulsed illumination with the 532-nm laser, while the light at $\lambda = 800$ nm is coupled to the waveguide [Fig. 3(a)]. Maximum optical transmission along the waveguide is achieved in the absence of any pre-synaptic pulse, whereas a transmission attenuation immediately occurs upon illumination with the pre-synaptic beam, recovering to its initial value after removal of the 532-nm light. The transmission attenuation of the post-synaptic 800-nm laser beam upon illumination of the waveguide with the pre-synaptic 532-nm laser comes from a contribution of transient photodarkening. Here, transient photodarkening can be understood as a reversible generation of absorbing color centers[25,32] taking place at the waveguide's input facet and it can be modulated upon a sequence of illumination cycles. Moreover, the illumination of the waveguide under different optical powers results in varying transmission attenuation levels, being an indication of the synaptic plasticity of the waveguide [Fig. 3(a)]. A maximum change in

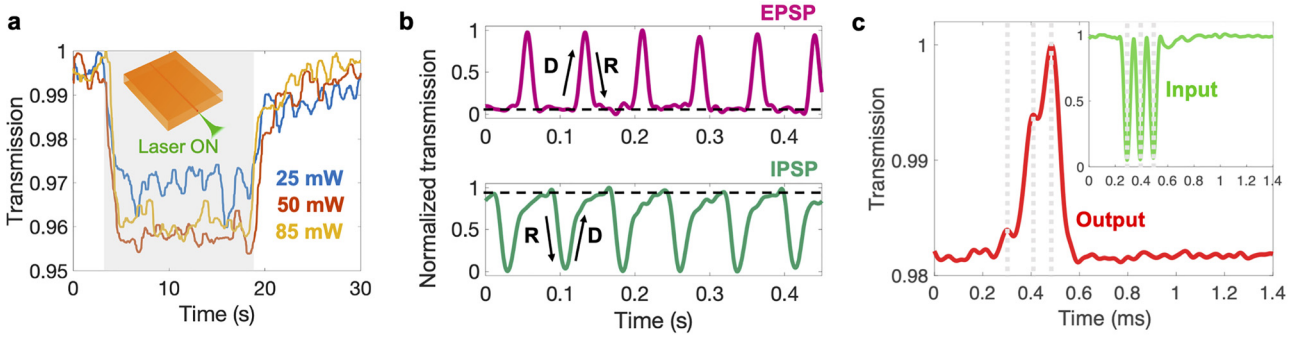

FIG. 3. (a) Transmission attenuation of the waveguide upon power modulation of the pre-synaptic beam. (b) EPSPs (upper panel) and IPSPs (lower panel) generated and transmitted along the waveguide (dashed black line: "resting potential," D: depolarization, R: repolarization). The EPSPs (IPSPs) are obtained from a power modulation of the pre-synaptic beam between the resting (inhibitory), 10 mW (25 mW), and the excitatory, 0 mW, potentials, for a duty cycle of 70% (30%) and a modulation frequency of 13 Hz. (c) Temporal summation (in red) of three individual input pulses (indicated by vertical gray dashed lines) generated in the waveguide upon power modulation of the pre-synaptic laser at ∼35 mW. The inset shows the input signal corresponding to the pre-synaptic laser beam (in green).

transmission of 4.5% is observed along the waveguide under illumination of pre-spike pulses carrying optical powers above ~50 mW, which is attributed to a saturation of the photoinduced changes. Larger attenuation in waveguide transmission might be achieved using light sources emitting near the ultraviolet spectral range (see the absorption spectrum of the pristine GLS glass in Fig. S1).

In biological systems, the transmission of information takes place in the form of action potentials, which are electrical signals originated from a change in voltage across the plasma membrane of any neuron. The action potentials propagate from the neuron's body to the axon terminal due to the allocation of voltage-gated ion channels along the axon, passing then across a synaptic junction and to a next neuron in the communication line. In the synaptic junction, a pre-synaptic neuron induces changes in the membrane potential of a post-synaptic neuron through the release of the electrical action potential in the form of chemical neurotransmitters.[26]

Typically, in the mammalian's nervous system, there are two types of action potentials: excitatory and inhibitory. The implementation of this bipolar mechanism depends on an increase (depolarization) or a decrease (repolarization) in the membrane voltage of the post-synaptic cell, which typically remains in a resting potential in the absence of any external stimulus.

Excitatory and inhibitory spiking activities, typical of biological neuronal systems, are mimicked in the photonic waveguide. Applying a power modulation of the pre-synaptic pulses at specific modulation rates allows to adjust the synaptic plasticity of the waveguide, giving rise to different excitatory and inhibitory post-synaptic potentials (EPSP and IPSP, respectively) [Fig. 3(b)]. These excitatory and inhibitory types of responses are representative features of short-term plasticity in neuroscience.[27] The duration of individual EPSPs and IPSPs generated in the waveguides is about 15 and 20 ms, respectively. These pulse durations are on the same order of magnitude as action potentials generated in animal's nervous cells where two main types of responses, caused through calcium and sodium ion channels, present duration times of 1 and 100 ms, respectively.[28] Considering a pre-synaptic firing rate of 13 Hz at a maximum power of 25 mW [Fig. 3(b)], the energy consumed by the artificial neuron for each fire-and-recovery cycle is ~1.9 J.

In addition to the generation of individual EPSPs and IPSPs, the integration in time of nonsimultaneous input unitary events plays an important role in biological neuronal networks for information transformation and processing. This biological feature, known as temporal summation, takes place when a target neuron receives repetitive inputs from a single axon terminal at short intervals, causing the inputs to summate temporarily.[28,29]

The waveguides reproduce temporal summations in a similar way as it happens in biological neurons. When a burst of pre-synaptic optical pulses carrying enough power is sent to the waveguide's input port, temporal summations of the individual pulses are generated and transmitted along the waveguide. In this case, the modulation of the pre-spike beam is applied between two power levels as in the case of generating EPSPs and IPSPs but at a larger photon flux (>25 mW).

The photonic temporal summation is illustrated in Fig. 3(c), where three input action potentials produce three EPSPs, but the second and third EPSPs are generated during the falling phase (repolarization) of the first and second EPSPs, respectively. Consequently, the individual spikes are integrated in time. This added optical transmission between successive post-spikes is analogous to the temporarily stored charge in the capacitance of post-synaptic biological membranes, which enables the addition of charge of a second EPSP to the charge of the first EPSPs, thus allowing for temporal summations.[30]

During information processing across the biological nervous system, the synaptic junctions connecting neurons are constantly strengthened (potentiated) and weakened (depressed). This ability of the brain to tune and undo neural connections is known as plasticity, and it controls how effectively pre-synaptic and post-synaptic neurons communicate with each other.[31] In this context, time plays an important role for neuron firing since the connection strength or synaptic weight depends on the relative timing between a pre-spike and a post-spike. Specifically, if a pre-spike occurs immediately before a post-spike, the change in the synaptic weight is strong, whereas if a pre-spike happens immediately after a post-spike the change in synaptic weight is weak. This principle is a form of Hebbian learning and is known as spike-timing-dependent plasticity (STDP) in biological neural networks.[31]

To mimic the STDP principles, the pre-synaptic beam is sent to the waveguide in the form of a burst of pulses oscillating between two power levels, following the same modulation cycles used previously to form EPSPs and IPSPs. This constant modulation mimics the strengthening and weakening cycles at the photonic synapse in terms of waveguide transmission [Fig. 4(a)]. While the photodarkening level keeps oscillating, the post-synaptic beam is launched into the waveguide, probing the level of photodarkening induced at the junction and simultaneously acting as a gate function for the pre-spike. The opening and closing of the post-spike can be applied anywhere in this constant cycle.

Various forms of STDP are collected in Fig. 4(b) at different pre- and post-synaptic relative timings Δt. The arrival time of the post-spike relative to the pre-spike at the photonic synaptic junction ($\Delta t = t_{post} - t_{pre}$) contributes to a change in waveguide transmission, going through potentiation and depression cycles. The relative change in waveguide transmission represents the changes in the neural connection strength (synaptic weight change) between pre-synaptic and post-synaptic beams. As in biological systems, the closer a pre-spike is to a post-spike ($\Delta t = 0$), the larger is the change in the synaptic weight. Conversely, the further a pre-spike is to a post-spike ($|\Delta t| \gg 0$), the smaller the change induced in the synaptic weight. Moreover, when the pre-spike beam precedes the post-spike beam, the synaptic weight depresses due to induced photodarkening, whereas when the post-spike precedes the pre-spike beam, the synaptic weight potentiates.

In summary, we have implemented a purely photonic axon in a compact waveguide platform via a single-step fabrication method. Through the application of external stimuli in the way of a modulation of light pulses, we have demonstrated a series of intra- and inter-neuronal communication protocols present in biological neural networks. This work contributes as a toolbox for emerging ultrafast and ultrabroad band photonic neuromorphic hardware with a fundamental building block realized in a single-step fabrication procedure, offering robustness and easy coupling mechanisms to other optical computing circuitry. Based on this proof-of-concept, future large-scale architectures can exploit the three-dimensional patterning and the parallel processing provided by the ultrafast laser inscription technique, where the effect of multiple interconnected waveguides could

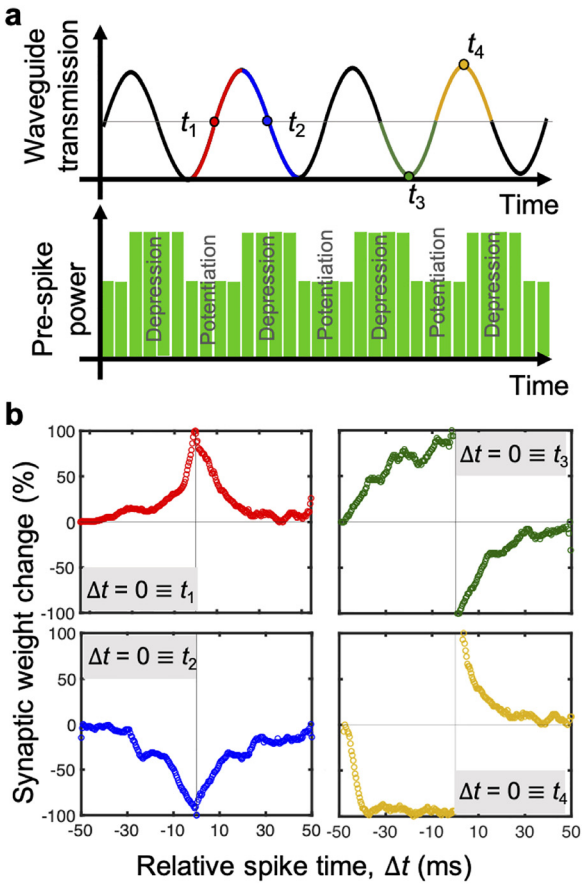

FIG. 4. (a) Pulsed light scheme of the pre-spike beam (lower panel) as a function of time used to induce plasticity at the photonic waveguide. Waveguide transmission upon modulation of the pre-spike beam (upper panel), where t_1, t_2, t_3, t_4 represent different timings along the modulation cycle. (b) Different Hebbian learning windows obtained at times indicated in (a): $\Delta t = 0 \equiv t_1, \Delta t = 0 \equiv t_2, \Delta t = 0 \equiv t_3, \Delta t = 0 \equiv t_4$.

play an important role in the connection strength of the photonic network.

See the supplementary material for a detailed description of the waveguide characterization losses.

The authors are grateful to Luigino Criante and Guglielmo Lanzani for access to the FemtoFab facility at CNST-IIT Milano for the laser fabrication experiments.

M.R. and C.S. acknowledge support from the Singapore Ministry of Education (Nos. MOE2011-T3-1-005 and MOE2016-T3-1-006) and the Agency for Science, Technology and Research (A*STAR, Grant No. A18A7b0058). IFN-CNR is grateful for support from the H2020 ERC project PAIDEIA (GA No. 816313) and H2020 Marie Curie ITN projects LasIonDef (GA No. 956387) and PHOTOTRAIN (GA No. 722591). A.G. is thankful for support from the Lombardy Region Project sPATIALS3 "Miglioramento delle produzioni agroalimentari e tecnologie innovative per un álimentazione più sana, sicura e sostenibile," cofunded by POR FESR 2014-2020 Call HUB Ricerca e Innovazione. S.M.E. is thankful for support from the CNR Short Term Mobility grant 2019.

DATA AVAILABILITY

The data that support the findings of this study are available from the corresponding author upon reasonable request.

REFERENCES

[1]J. Zhu, T. Zhang, Y. Yang, and R. Huang, "A comprehensive review on emerging artificial neuromorphic devices," Appl. Phys. Rev. **7**, 011312 (2020).
[2]P. R. Prucnal and B. J. Shastri, *Neuromorphic Photonics* (CRC Press, 2017).
[3]R. A. Nawrocki, R. M. Voyles, and S. E. Shaheen, "A mini review of neuromorphic architectures and implementations," IEEE Trans. Electron Devices **63**, 3819–3829 (2016).
[4]Z. Wang, S. Joshi, S. E. Savel'ev, H. Jiang, R. Midya, P. Lin, M. Hu, N. Ge, J. P. Strachan, Z. Li *et al.*, "Memristors with diffusive dynamics as synaptic emulators for neuromorphic computing," Nat. Mater. **16**, 101–108 (2017).
[5]S. Majumdar, H. Tan, Q. H. Qin, and S. van Dijken, "Energy-efficient organic ferroelectric tunnel junction memristors for neuromorphic computing," Adv. Electron. Mater. **5**, 1800795 (2019).
[6]Y. Li, Z. Wang, R. Midya, Q. Xia, and J. J. Yang, "Review of memristor devices in neuromorphic computing: Materials sciences and device challenges," J. Phys. D **51**, 503002 (2018).
[7]E. Goi, Q. Zhang, X. Chen, H. Luan, and M. Gu, "Perspective on photonic memristive neuromorphic computing," PhotoniX **1**, 1–26 (2020).
[8]C.-S. Yang, D.-S. Shang, N. Liu, E. J. Fuller, S. Agrawal, A. A. Talin, Y.-Q. Li, B.-G. Shen, and Y. Sun, "All-solid-state synaptic transistor with ultralow conductance for neuromorphic computing," Adv. Funct. Mater. **28**, 1804170 (2018).
[9]I. Sanchez Esqueda, X. Yan, C. Rutherglen, A. Kane, T. Cain, P. Marsh, Q. Liu, K. Galatsis, H. Wang, and C. Zhou, "Aligned carbon nanotube synaptic transistors for large-scale neuromorphic computing," ACS Nano **12**, 7352–7361 (2018).
[10]S. Jiang, S. Nie, Y. He, R. Liu, C. Chen, and Q. Wan, "Emerging synaptic devices: From two-terminal memristors to multiterminal neuromorphic transistors," Mater. Today Nano **8**, 100059 (2019).
[11]V. K. Sangwan and M. C. Hersam, "Neuromorphic nanoelectronic materials," Nat. Nanotechnol. **15**, 517–528 (2020).
[12]S. Dai, Y. Zhao, Y. Wang, J. Zhang, L. Fang, S. Jin, Y. Shao, and J. Huang, "Recent advances in transistor-based artificial synapses," Adv. Funct. Mater. **29**, 1903700 (2019).
[13]P. Minzioni, C. Lacava, T. Tanabe, J. Dong, X. Hu, G. Csaba, W. Porod, G. Singh, A. E. Willner, A. Almaiman *et al.*, "Roadmap on all-optical processing," J. Opt. **21**, 063001 (2019).
[14]B. Gholipour, P. Bastock, C. Craig, K. Khan, D. Hewak, and C. Soci, "Amorphous metal-sulphide microfibers enable photonic synapses for brain-like computing," Adv. Opt. Mater. **3**, 635–641 (2015).
[15]Z. Cheng, C. Ríos, W. H. Pernice, C. D. Wright, and H. Bhaskaran, "On-chip photonic synapse," Sci. Adv. **3**, e1700160 (2017).
[16]A. N. Tait, T. F. De Lima, E. Zhou, A. X. Wu, M. A. Nahmias, B. J. Shastri, and P. R. Prucnal, "Neuromorphic photonic networks using silicon photonic weight banks," Sci. Rep. **7**, 7430 (2017).
[17]I. Chakraborty, G. Saha, A. Sengupta, and K. Roy, "Toward fast neural computing using all-photonic phase change spiking neurons," Sci. Rep. **8**, 12980 (2018).
[18]M. R. Vázquez, V. Bharadwaj, B. Sotillo, S.-Z. A. Lo, R. Ramponi, N. I. Zheludev, G. Lanzani, S. M. Eaton, and C. Soci, "Optical NP problem solver on laser-written waveguide platform," Opt. Express **26**, 702–710 (2018).
[19]X.-Y. Xu, X.-L. Huang, Z.-M. Li, J. Gao, Z.-Q. Jiao, Y. Wang, R.-J. Ren, H. Zhang, and X.-M. Jin, "A scalable photonic computer solving the subset sum problem," Sci. Adv. **6**, eaay5853 (2020).
[20]K. Wu, J. G. De Abajo, C. Soci, P. P. Shum, and N. I. Zheludev, "An optical fiber network oracle for NP-complete problems," Light **3**, e147 (2014).
[21]C. Roques-Carmes, Y. Shen, C. Zanoci, M. Prabhu, F. Atieh, L. Jing, T. Dubček, C. Mao, M. R. Johnson, V. Čeperić *et al.*, "Heuristic recurrent algorithms for photonic Ising machines," Nat. Commun. **11**, 249 (2020).

[22]K. M. Davis, K. Miura, N. Sugimoto, and K. Hirao, "Writing waveguides in glass with a femtosecond laser," Opt. Lett. **21**, 1729–1731 (1996).
[23]R. Osellame, G. Cerullo, and R. Ramponi, *Femtosecond Laser Micromachining: Photonic and Microfluidic Devices in Transparent Materials* (Springer Science & Business Media, 2012), Vol. 123.
[24]M. R. Vázquez, B. Sotillo, S. Rampini, V. Bharadwaj, B. Gholipour, P. Fernández, R. Ramponi, C. Soci, and S. M. Eaton, "Femtosecond laser inscription of nonlinear photonic circuits in gallium lanthanum sulphide glass," J. Phys. **1**, 015006 (2018).
[25]A. Ganjoo, K. Shimakawa, K. Kitano, and E. Davis, "Transient photodarkening in amorphous chalcogenides," J. Non-Cryst. Solids **299–302**, 917–923 (2002).
[26]D. E. Sadava, D. M. Hillis, H. C. Heller, and M. Berenbaum, *Life: The Science of Biology* (Macmillan, 2009), Vol. 2.
[27]G. T. Neske, S. L. Patrick, and B. W. Connors, "Contributions of diverse excitatory and inhibitory neurons to recurrent network activity in cerebral cortex," J. Neurosci. **35**, 1089–1105 (2015).
[28]J. C. Cheng, N. Erpelding, A. Kucyi, D. D. DeSouza, and K. D. Davis, "Individual differences in temporal summation of pain reflect pronociceptive and antinociceptive brain structure and function," J. Neurosci. **35**, 9689–9700 (2015).
[29]J. C. Magee, "Dendritic I_h normalizes temporal summation in hippocampal CA1 neurons," Nat. Neurosci. **2**, 508–514 (1999).
[30]J.-Y. Sun and L.-G. Wu, "Fast kinetics of exocytosis revealed by simultaneous measurements of presynaptic capacitance and postsynaptic currents at a central synapse," Neuron **30**, 171–182 (2001).
[31]D. O. Hebb, *The Organization of Behavior: A Neuropsychological Theory* (Psychology Press, 2005).
[32]D. C. Sati, A. Dahshan, and P. Sharma, "Photoinduced effects for amorphous chalcogenide semiconductors," Appl. Mater. Today **17**, 142–158 (2019).
[33]D. W. Hewak, D. Brady, R. J. Curry, G. Elliott, C.-C. Huang, M. Hughes, K. Knight, A. Mairaj, M. Petrovich, R. Simpson *et al.*, *Chalcogenide Glasses for Photonics Device Applications* (University of Southampton, 2010).